ATLAS NOTE

ATLAS-CONF-2011-156

November 14, 2011

Constraining the gauge-mediated Supersymmetry breaking model in final states with two leptons, jets and missing transverse momentum with the ATLAS experiment at $\sqrt{s}$ = 7 TeV

The ATLAS Collaboration

Abstract

This note describes a new interpretation of a search for Supersymmetry in final states with exactly two oppositely charged leptons, jets and missing transverse momentum within the gauge-mediated Supersymmetry breaking model. The obtained exclusions significantly extend existing limits.

1 Introduction

Supersymmetry (SUSY) [1], as many other extensions to the Standard Model (SM), predicts the existence of coloured particles, squarks ($\tilde{q}$) and gluinos ($\tilde{g}$), that could be copiously produced at the LHC. In gauge-mediated supersymmetry breaking (GMSB) models [2–8], the squarks and gluinos decay directly or through steps into the next-to-lightest SUSY particle (NLSP), which further decays into its SM partner and the lightest supersymmetric particle (LSP), a nearly massless gravitino ($\tilde{G}$). Possible NLSP candidates are the lightest stau ($\tilde{\tau}_1$), right handed sleptons ($\tilde{\ell}_R$), the lightest neutralino ($\tilde{\chi}_1^0$) or sneutrinos ($\tilde{\nu}$). The gravitino escapes detection and gives rise to missing transverse momentum, $E_{\mathrm{T}}^{\mathrm{miss}}$. Depending on the nature of the NLSP, the final states contain $E_{\mathrm{T}}^{\mathrm{miss}}$, jets from the $\tilde{q}$ and $\tilde{g}$ decays and either leptons (e/μ), τ leptons, photons or neutrinos. Previous results on GMSB scenarios have been reported by the LEP [9–12], Tevatron [13, 14] and LHC experiments [15, 16]. While the LEP limits are provided for exactly the same model considered in this note, the Tevatron and LHC results are not directly applicable here.

This note reports on the interpretation within the GMSB scenario of the ATLAS dilepton SUSY analysis [17] based on 1.04 fb^{-1} of data collected with the ATLAS detector at a centre-of-mass energy of $\sqrt{s}$ = 7 TeV. The signal selection criteria are taken without modification from the search for SUSY in dileptonic final states. From the three signal regions for opposite sign (OS) leptons discussed in Ref. [17], the 3 jets+$E_{\mathrm{T}}^{\mathrm{miss}}$ signal region[1] is used for the GMSB interpretation discussed here, since it provides the best sensitivity for all signals studied. The background estimation and all background related uncertainties are also taken from Ref. [17].

In GMSB models, the messenger fields, which exist at a scale M_{mes} ($\ll M_{Pl} = \sqrt{\frac{\hbar c}{G}}$), transmit the breaking of SUSY from the hidden to the accessible sector. Assuming a minimal GMSB model, these messenger fields form a complete representation of $SU(5)$ and thus preserve the unification of the gauge coupling constants. The minimal GMSB model can be described by six parameters: Λ, M_{mes}, N_5, $\tan\beta$, sign(μ) and C_{grav}, where Λ is the SUSY breaking scale felt by the low energy sector, M_{mes} is the mass scale of the messenger fields, which needs to be greater than Λ to avoid charge and color breaking in the messenger sector and N_5 represents the number of messenger fields. The ratio of the vacuum expectation values of the two Higgs doublets is given by $\tan\beta$, while sign(μ) is the sign of the Higgsino mass term. Finally, C_{grav} is the scale of the gravitino coupling.

The sparticle masses at the breaking scale Λ are evolved via the renormalization group equations to the weak scale and lead to a linear dependence of these masses on Λ. Typical values of Λ are 10–100 TeV. Gaugino and sfermion masses are proportional to N_5 and $\sqrt{N_5}$, respectively. The gravitino coupling determines the lifetime of the next-to-lightest supersymmetric particle.

2 Characteristics of the GMSB scenario

In this note, results are interpreted as function of Λ and $\tan\beta$ for fixed values of M_{mes} = 250 TeV, N_5 = 3, sign(μ) positive and C_{grav} = 1. The calculation of the sparticle masses at the weak scale is done with ISAJET [18]. Current limits from LEP for this scenario exclude values of Λ up to 26 TeV irrespective of $\tan\beta$ [12].

The GMSB signal samples are generated with HERWIG++ [19] and the corresponding cross sections are determined at next-to-leading order (NLO) using PROSPINO [20–24] and CTEQ6.6 parton distribution functions (PDF) [25]. All simulated events are produced using an ATLAS parameter tune [26] and a GEANT4 [27] based detector simulation [28]. To take into account differing pileup conditions depending on the setup of the LHC machine, Monte Carlo (MC) simulated events are reweighted according to the

[1] The signal region is called OS-SR 2 in Ref. [17].

mean expected number of interactions per bunch crossing.

Different SUSY particles can take the role of the NLSP depending on the choice of Λ and $\tan\beta$. At low values of Λ, the lightest neutralino is the NLSP while for values above 20 TeV either the lightest stau $\tilde{\tau}_1$ or right-handed slepton $\tilde{\ell}_R$ are the NLSP. The $\tilde{\tau}_1$ is lighter than the $\tilde{\ell}_R$ for large values of $\tan\beta$, while the situation is reversed for low $\tan\beta$. The regions for the various NLSP's are depicted in Fig. 1.

The branching ratios of $\tilde{\chi}_1^0$ to $\tilde{\tau}_1\tau$ and to $\tilde{\ell}_R\ell$ depicted in Fig. 2 reflect this transition. In the slepton NLSP region, the sleptons directly decay to a lepton and a gravitino, while in the stau NLSP region, they decay into $\tilde{\tau}_1\tau\ell$ as shown in Fig. 3. The staus always decay into a τ lepton and a gravitino, both in the stau and slepton NLSP region. Therefore, the leptons originate either directly from $\tilde{e}_R/\tilde{\mu}_R$ or from leptonic τ decays, depending on $\tan\beta$, with some smaller contribution from the decays of heavier gauginos. Given these decay properties, a dileptonic selection is expected to provide good sensitivity for a GMSB signal. In the slepton NLSP region, the same flavour final states yield higher efficiencies since for each decay chain involving a slepton two oppositely charged leptons of the same flavour are produced. If the decays proceed via staus to τ leptons and thus electrons and muons stem from the leptonic τ decays, the $e\mu$ final state gains in sensitivity due to increased branching fraction in opposite sign opposite flavour states.

3 Analysis

The data used in this analysis were collected between March and June 2011 at a centre-of-mass energy of 7 TeV corresponding to an integrated luminosity of 1.04 ± 0.04 fb^{-1}.

Electrons need to fulfil kinematic requirements on the transverse energy of $E_{\mathrm{T}} > 20$ GeV and $|\eta| < 2.47$. If the electron candidate overlaps with a jet within $0.2 < \Delta R < 0.4$, where $\Delta\mathcal{R} = \sqrt{(\Delta\eta)^2 + (\Delta\phi)^2}$, this candidate is removed from the list of electrons. If the distance is smaller, the electron is retained and the jet is discarded instead. The electron must be isolated and the E_{T} requirement is raised to 25 GeV if the electron is the leading lepton in the event.

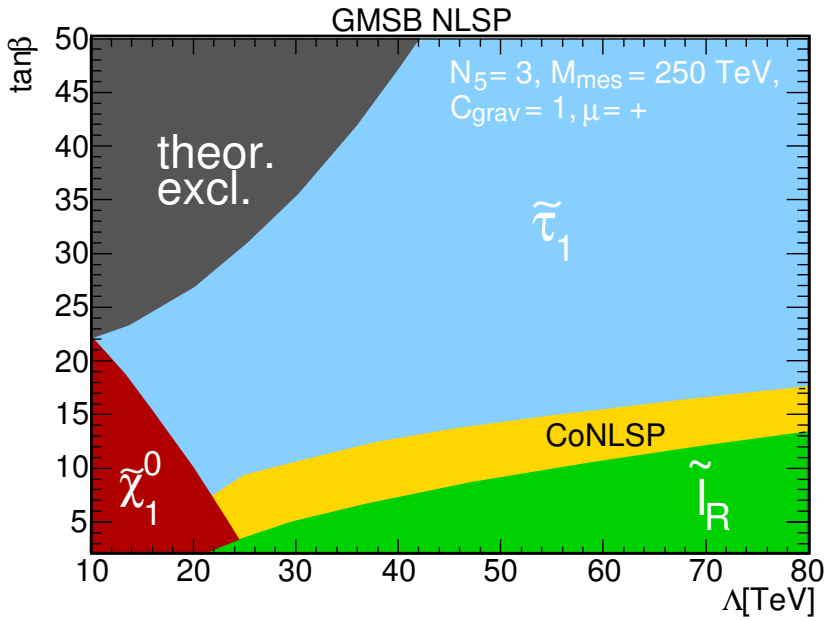

Figure 1: Overview of the regions with different NLSP's in the Λ-$\tan\beta$ plane for the gauge-mediated SUSY breaking model. The CoNLSP region denotes the parameter space where $\tilde{\tau}_1$ and $\tilde{\ell}_R$ are nearly mass degenerate.

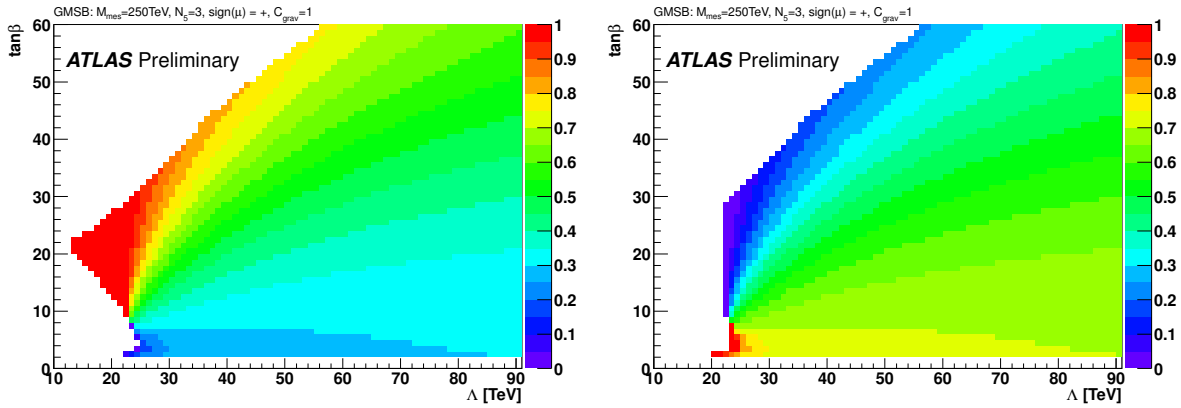

Figure 2: Branching Ratio of $\tilde{\chi}_1^0$ to $\tilde{\tau}_1\tau$ (left) and to $\tilde{\ell}_R\ell$ (right) as a function of Λ and $\tan\beta$.

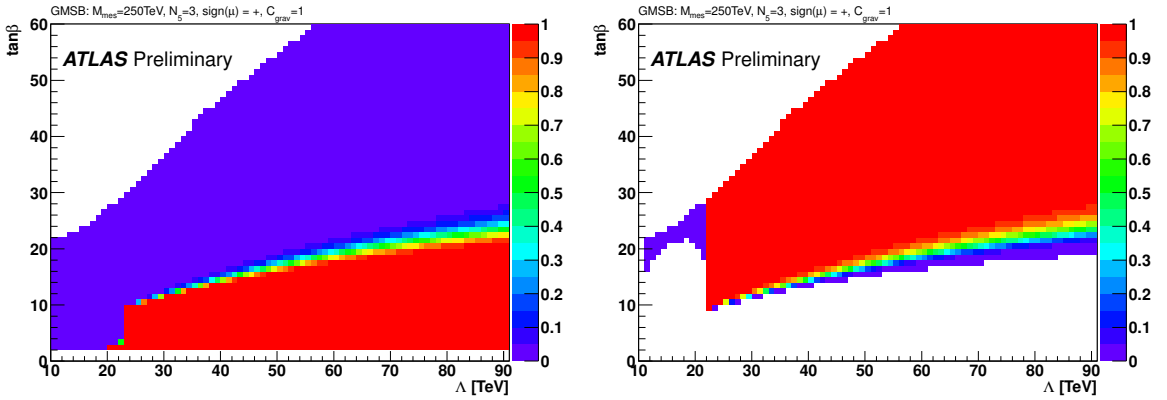

Figure 3: Branching Ratio of $\tilde{\ell}_R$ to $\tilde{G}\ell$ (left) and to $\tilde{\tau}_1\tau\ell$ (right) as a function of Λ and $\tan\beta$.

Muons are required to have a transverse momentum of $p_{\mathrm{T}} > 10$ GeV and $|\eta| < 2.4$. Only muons isolated from jets ($\Delta\mathcal{R} < 0.4$) and isolated in the inner tracking detector are taken into account. In the case of the muon being the highest p_{T} lepton in the event, the p_{T} requirement is tightened to > 20 GeV.

Jets are reconstructed using an anti-k_t jet algorithm [29] with a radius parameter of 0.4. Kinematic requirements of $E_{\mathrm{T}} > 20$ GeV and $|\eta| < 2.8$ are applied to all jets.

The missing transverse momentum is the negative vectorial E_{T} sum of reconstructed objects in the event, including the jets, the two signal leptons, any additional identified non-isolated muons, and topological calorimeter clusters up to $|\eta| < 4.5$ not belonging to any of the aforementioned object types. A more detailed description of the object selection is given in Ref. [17].

The event selection starts by requiring a primary vertex with at least five associated tracks. The kinematic selection requires exactly two leptons of opposite charge. Events with additional leptons are discarded. In the case of dielectron (ee) and dimuon ($\mu\mu$) final states, events must satisfy a single electron and single muon trigger condition, respectively. For mixed lepton flavour ($e\mu$) either a single electron or single muon trigger is used, depending on the transverse momentum of the leptons.

A lower cut of 12 GeV on the invariant dilepton mass, $m_{\ell\ell}$, is applied to remove low-mass dilepton resonances. The final signal region is defined by requirements on the missing transverse momentum to account for the escaping LSP and by a jet selection to reflect the presence of jets in strong production of SUSY particles: $E_{\mathrm{T}}^{\mathrm{miss}} > 220$ GeV and at least three jets, with $E_{\mathrm{T}} > 80$ GeV for the leading jet, and

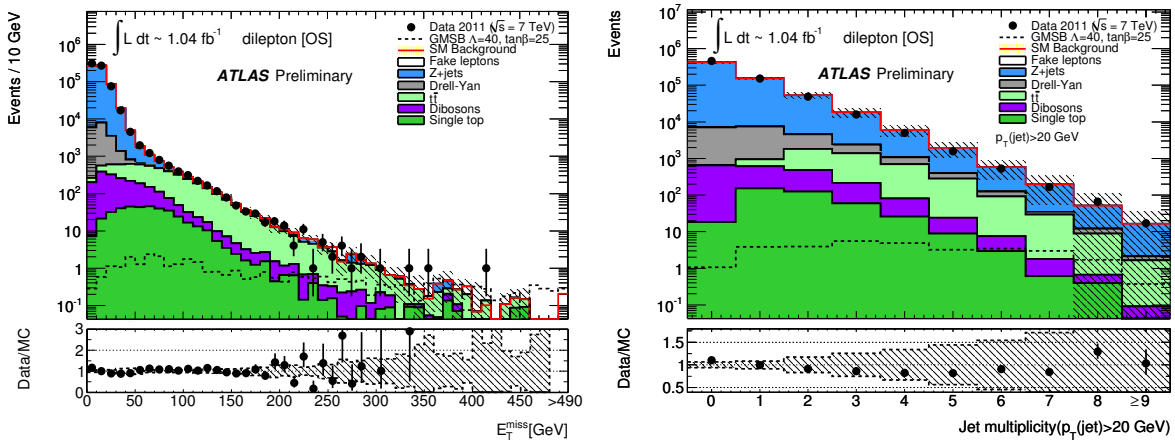

Figure 4: Distribution of the missing transverse momentum (left) and the jet multiplicity (right) after requiring two oppositely charged leptons. The hatched bands reflect the statistical and systematic uncertainties. The expected contribution from a GMSB signal with $\Lambda = 40$ TeV and $\tan\beta = 25$ is also shown as a black dashed line.

40 GeV for the other jets. Figure 4 shows the $E_{\mathrm{T}}^{\mathrm{miss}}$ and jet multiplicity distributions before applying the $E_{\mathrm{T}}^{\mathrm{miss}}$ and jet requirements. A good description of the data by the MC simulation is observed.

The backgrounds are determined in dedicated control regions and the MC simulation is used to extrapolate from these control regions to the signal region. The main background components are $t\bar{t}$ and Z/γ^*+jets production. The $t\bar{t}$ control region is defined using a kinematic tagger, while Z/γ^*+jets events are selected at low $E_{\mathrm{T}}^{\mathrm{miss}}$ in a window around the Z mass. A detailed discussion of the background determination techniques is provided in Ref. [17].

4 Systematic uncertainties

Different sources of systematic uncertainties impact the prediction of SUSY and background events in the signal region. The main sources are the jet energy scale (JES) and resolution (JER), cross section and MC modelling uncertainties. In addition, the limited number of MC events in the signal region and data events in the control regions gives rise to sizable uncertainties on the final background prediction.

The JES and JER uncertainties are estimated by varying the nominal values within their uncertainties [30], resulting in changes in the background prediction of 6% and 11%, respectively. The MC modelling and amount of ISR/FSR in $t\bar{t}$ events is studied using different generators. The related uncertainties are found to be 13% for the generator and 16% for the ISR/FSR variation. The uncertainty due to limited statistics in the background determination methods is 10% for the $t\bar{t}$ background, while the uncertainty due to luminosity is 3.7% [31]. Lepton uncertainties from identification and resolution are negligible.

The scale and PDF uncertainties of the GMSB signal are studied using PROSPINO[2]. In addition to the variations of the eigenvectors of the PDF, also the uncertainty related to the variation of α_s is taken into account. The PDF uncertainties are found to be 10% at low values of Λ rising to 30% at high values of either Λ or $\tan\beta$. This increase in the uncertainty is related to a rise in the masses of the gluinos and squarks with Λ. With higher masses, larger x values of the PDF are probed which results in larger uncertainties due the larger errors of the PDF at high x.

[2]It is necessary to rescale the 90% CL uncertainties provided by PROSPINO to 68% CL.

Table 1: Number of expected background events and events observed in the data for the three different final states in the signal region using the selection of Ref. [17]. The first errors are statistical and the second systematic. The negative expected number of $\mu\mu$ fakes is an artefact of the matrix method used for this background determination.

	ee	$e\mu$	$\mu\mu$
$t\bar{t}$	1.4±0.1±0.3	3.9±0.3±1.0	2.6±0.2±0.6
Z/γ^*+jets	0.45±0.23±0.44	0.84±0.59±0.32	0.27±0.14±0.27
Fakes	0.01±0.14±0.003	2.8±1.6±2.1	-0.13±0.04±0.05
Dibosons	-	0.03±0.03±0.03	0.24±0.21±0.02
Single-top	0.05±0.10±0.02	0.39±0.16±0.25	0.09±0.15±0.08
Total	1.9±0.3±0.8	7.9±1.8±2.5	3.2±0.4±0.9
Data	3	9	5

The uncertainties from scale variations depend on the SUSY particles produced in the hard interaction. For strong production, typical uncertainties are around 20% with a small increase with increasing Λ. For associated production of squarks and gauginos, the uncertainties lie between 20 and 25%, while they are small (2–5%) for gaugino pair production. The JES and JER uncertainties are found to range from 10% to 20%. The limited MC statistics leads to uncertainties of 7% at high values of Λ and increase up to 40% at low values of Λ as well as close to the border of the theoretically inaccessible area.

5 Results and interpretation

In the following, the results from Ref. [17] are used for the GMSB interpretation. After applying all selection requirements, the total number of expected background events are compared to the number of events observed in data. The total background expectation is 1.9±0.3(stat.)±0.8(syst.) events, 7.9±1.8(stat.)±2.5(syst.) events and 3.2±0.4(stat.)±0.9(syst.) events in the ee, $e\mu$ and $\mu\mu$ channel, respectively, while three, nine and five events are observed in the data. In all three channels, the dominant contributions stem from $t\bar{t}$ events, which make up between 50 and 80% of the total expected SM background. Also Z/γ^*+jets events yield a sizeable contribution to all channels. In addition, contributions from processes with misidentified leptons, dominated by semileptonic $t\bar{t}$ decays, are important in the $e\mu$ channel. A detailed overview of the expected backgrounds is given in Table 1.

The signal selection efficiency depends on the production mechanism. The highest selection efficiencies are obtained for the squark-gaugino production channel with values reaching up to 30%. In addition, squark-gluino and gluino pair production also yield good efficiencies (up to 20%) due the larger number of expected jets in the final state, while squark-(anti)squark and gaugino gaugino production only yield small signal efficiencies. The selection efficiencies for $\tilde{g}\tilde{g}$, $\tilde{q}\tilde{g}$, $\tilde{q}\tilde{\chi}$ and $\tilde{\chi}\tilde{\chi}$ production are shown in Fig. 5. To quantify the importance of the different production channels, their relative contributions to the total expected signal abundance are displayed in Fig. 6. The overall numbers of expected signal events for the three different final states in the Λ-tanβ plane are shown in Fig. 7.

Since there is no evidence for a signal the results are used to set limits on GMSB production. A profile likelihood technique [32], based on the CL_s method [33], is used to extract limits at 95% Confidence Level (CL) in the Λ-tanβ plane. The expected and observed exclusion contours for the individual channels are given in Fig. 8. The shape of the exclusion limits reflects the characteristics of the GMSB signal discussed in Section 2. At low values of tanβ, the ee and $\mu\mu$ final states yield better limits compared to the $e\mu$ final state. With increasing values of tanβ, the exclusion reach of the $e\mu$ selection gets

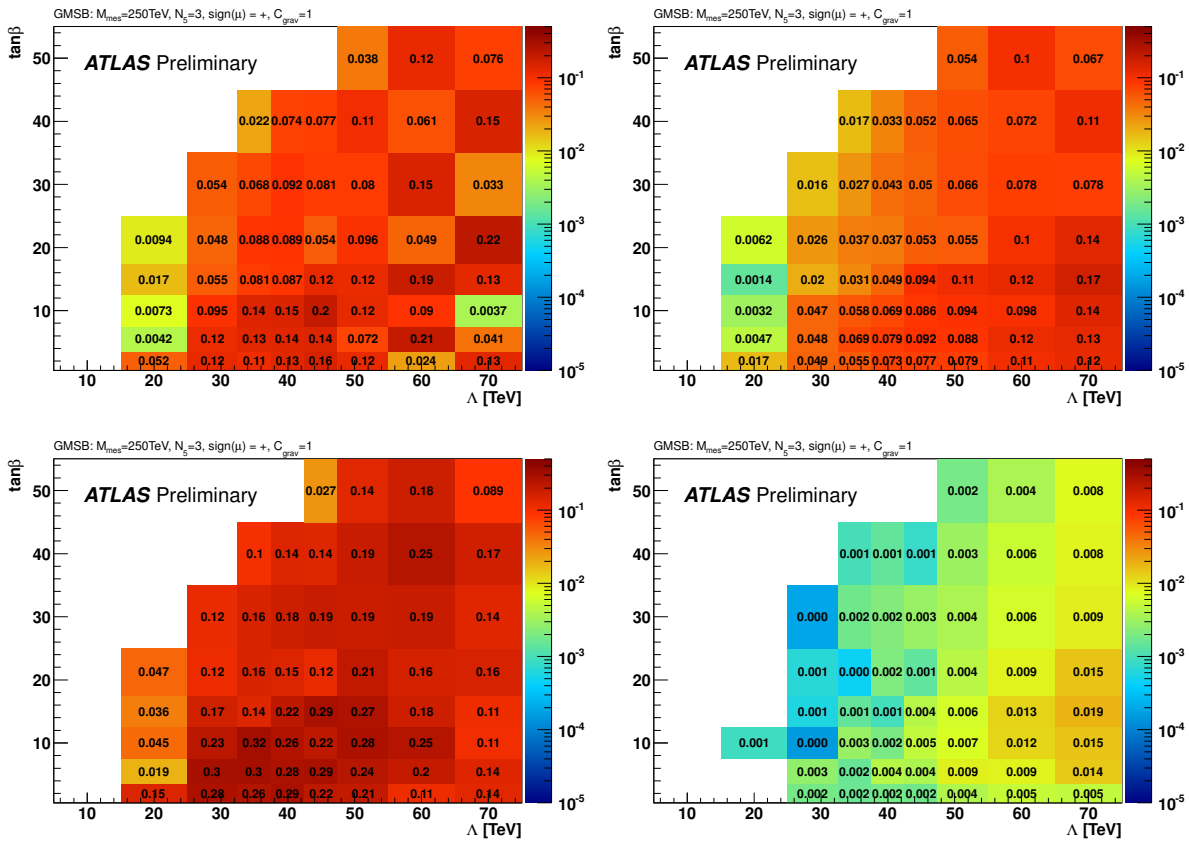

Figure 5: Signal selection efficiency × acceptance as function of Λ and $\tan\beta$ for gluino-gluino (top left), squark-gluino (top right), squark-gaugino (bottom left) and gaugino-gaugino production (bottom right).

better, reflecting the transition from slepton to stau NLSP. It can also be observed that the $\mu\mu$ selection performs better in this region compared to the ee channel, since the $\mu\mu$ selection with a lower lepton p_{T} threshold is more efficient in selecting the softer leptons from the leptonic τ decays. This is further illustrated further in Fig. 9 which shows the p_{T} distribution of the second leading muon for data and the expected SM backgrounds.

The combination of all three final states is shown in Fig. 10. The analysis excludes GMSB production with Λ values of 20-35 TeV for $\tan\beta$ values up to 30. For $\tan\beta$ values below 10, the exclusion region extends to $\Lambda = 40$ TeV. In all areas, the observed limit is weaker compared to the expected one, since in all three selections, the number of events observed in the data slightly exceeds the background predictions.

6 Summary and conclusion

In this note, the dilepton analysis with exactly two OS leptons, at least three jets and $E_{\mathrm{T}}^{\mathrm{miss}}$ is interpreted in the minimal GMSB scenario. Using 1.04 fb^{-1} of ATLAS data recorded at a centre-of-mass energy of 7 TeV, no excess above the Standard Model prediction is observed. The exclusion limits obtained improve significantly on already existing limits and probe GMSB production for values up to $\Lambda = 40$ TeV.

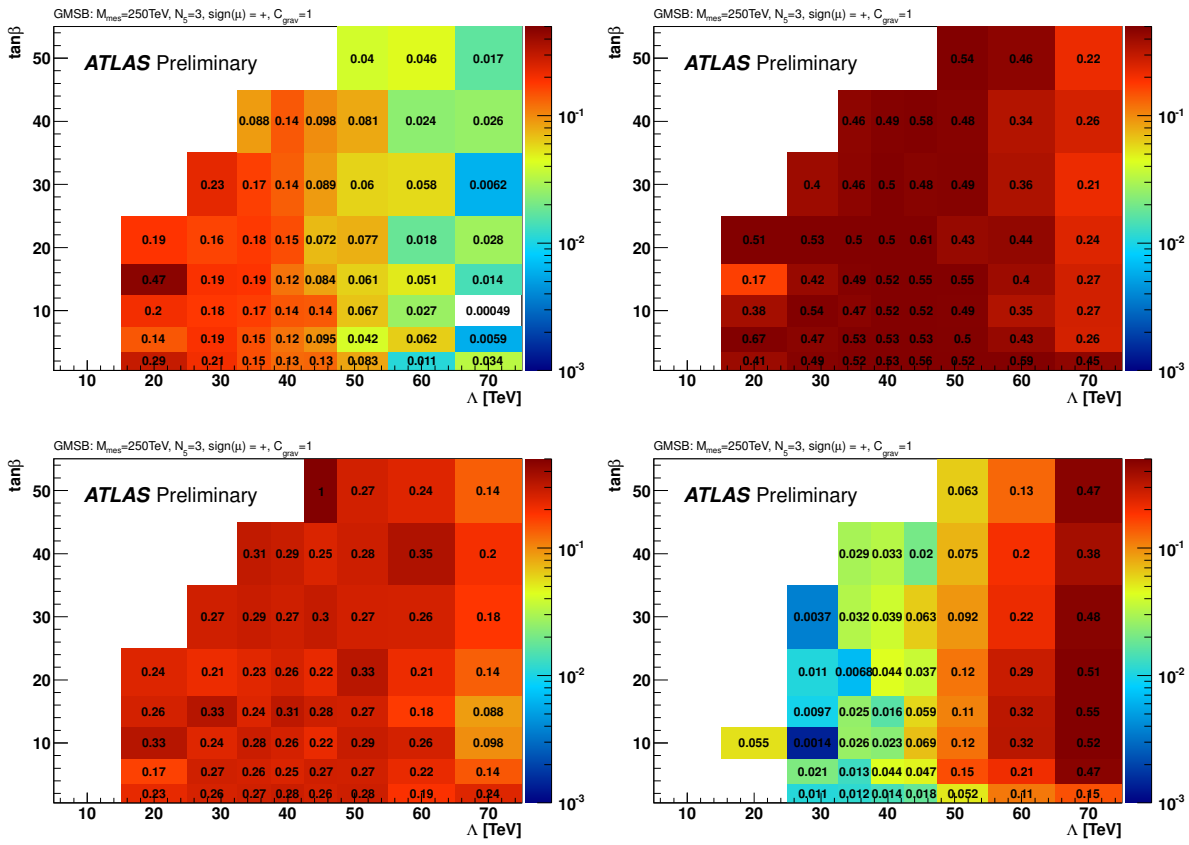

Figure 6: Relative contribution to the signal expectation from gluino-gluino (top left), gluino-squark (top right), squark-gaugino (bottom left) and gaugino-pair production (bottom right) as a function of Λ and $\tan\beta$.

References

[1] Yu.A. Golfand and E.P. Likhtman, JETP Lett. **13** (1971) 323; A. Neveu and J.H. Schwartz, Nucl. Phys. B **31** (1971) 86; A. Neveu and J.H. Schwartz, Phys. Rev. D **4** (1971) 1109; P. Ramond, Phys. Rev. D **3** (1971) 2415; D.V. Volkov and V.P. Akulov, Phys. Lett. B **46** (1973) 109; J. Wess and B. Zumino, Phys. Lett. B **49** (1974) 52; J. Wess and B. Zumino, Nucl. Phys. B **70** (1974) 39.

[2] L. Alvarez-Gaume, M. Claudson, and M. Wise, *Low-energy supersymmetry*, Nucl. Phys. **B207** (1982) 96.

[3] M. Dine, W. Fischler, and M. Srednicki, *Supersymmetric technicolor*, Nucl. Phys. **B189** (1981) 575.

[4] S. Dimopoulos and S. Raby, *Supercolor*, Nucl. Phys. **B192** (1981) 353.

[5] C. R. Nappi and B. A. Ovrut, *Supersymmetric extension of the SU(3)×SU(2)×U(1) Model*, Phys. Lett. **B113** (1982) 175.

[6] M. Dine and A. Nelson, *Dynamical supersymmetry breaking at low-energies*, Phys. Rev. **D48** (1993) 1277, `hep-ph/9303230`.

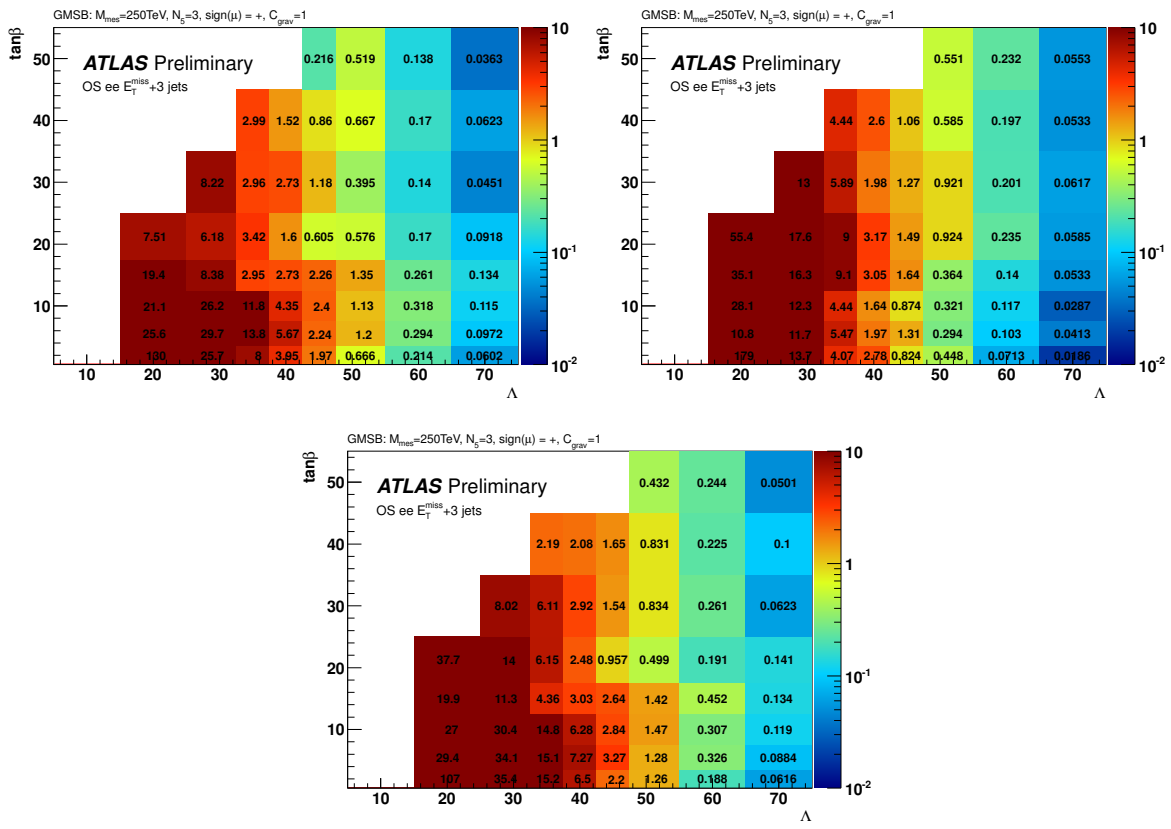

Figure 7: Number of expected signal events as function of Λ and $\tan\beta$ for the *ee* (top left), $e\mu$ (top right), and $\mu\mu$ selection (bottom).

[7] M. Dine, A. Nelson, and Y. Shirman, *Low-energy dynamical supersymmetry breaking simplified*, Phys. Rev. **D51** (1995) 1362, hep-ph/9408384.

[8] M. Dine, A. Nelson, Y.Nir, and Y. Shirman, *New tools for low-energy dynamical supersymmetry breaking*, Phys. Rev. **D53** (1996) 2658, hep-ph/9507378.

[9] ALEPH Collaboration, R. Barate et al., *Single- and multi-photon production in e^+e^- collisions at $\sqrt{s}$ up to 209 GeV*, Eur. Phys. J **C28** (2003) 1.

[10] DELPHI Collaboration, J. Abdallah et al., *Photon Events with Missing Energy in e^+e^- collisions at $\sqrt{s}$ = 130 to 209 GeV*, Eur. Phys. J **C38** (2005) 394–411.

[11] L3 Collaboration, P. Achard et al., *Single- and Multi-Photon events with Missing Energy in e^+e^- Collisions at LEP*, Phys. Lett. **B587** (2004) 16.

[12] OPAL Collaboration, G. Abbiendi et al., *Multi-Photon Events with Large Missing Energy in e^+e^- Collisions at $\sqrt{s}$ = 192-209 GeV*, Phys. Lett. **B602** (2004) 167–179.

[13] CDF Collaboration, T. Aaltonen et al., *Search for Supersymmetry with Gauge-Mediated Breaking in Diphoton Events with Missing Transverse Energy at CDF II*, Phys. Rev. Lett. **105** (2010) 011801, hep-ex/0910.3606.

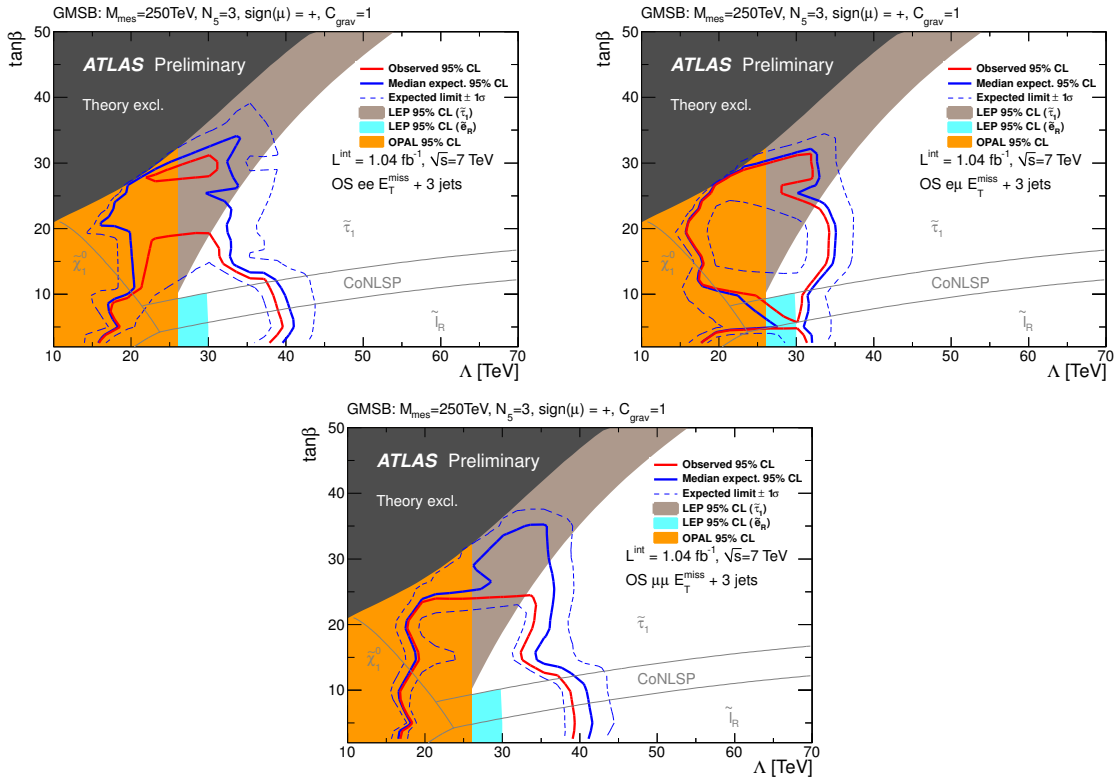

Figure 8: Observed (red) and expected (blue) 95% CL exclusion limits as function of Λ and $\tan\beta$ for the *ee* (top left), $e\mu$ (top right) and $\mu\mu$ final state (bottom). The ± 1 σ lines (dashed) are also shown. The different NLSP regions as well as the region excluded by theory and LEP experiments are indicated as well. The limit contour in the region with values of Λ between 10 and 20 TeV is affected by limited MC statistics. The CoNLSP region denotes the parameter space where $\tilde{\tau}_1$ and $\tilde{\ell}_R$ are nearly mass degenerate.

[14] DØ Collaboration, V. Abazov et al., *Search for Diphoton Events with Large Missing Transverse Energy in 6.3 fb^{-1} of $p\bar{p}$ Collisions at $\sqrt{s}$ = 1.96 TeV*, Phys. Rev. Lett. **105** (2010) 221802, hep-ex/1008.2133.

[15] CMS Collaboration, *Search for Supersymmetry in Events with Photons, Jets and Missing Energy*, CMS-PAS-SUS-11-009.

[16] ATLAS Collaboration, *Search for Heavy Long-Lived Charged Particles with the ATLAS detector in pp collisions at $\sqrt{s}$ = 7 TeV*, arXiv:1106.4495 [hep-ex].

[17] ATLAS Collaboration, *Searches for supersymmetry using final states with two leptons and missing transverse momentum with the ATLAS detector in $\sqrt{s}$ = 7 TeV proton-proton collisions*, arXiv:1110.6189 [hep-ex].

[18] H. Baer, F. E. Paige, S. D. Protopopescu, and X. Tata, *Simulating Supersymmetry with ISAJET 7.0 / ISASUSY 1.0*, arXiv:hep-ph/9305342 [hep-ph].

[19] M. Bahr et al., Eur. Phys. J. C **58** (2008) 639.

[20] W. Beenakker, R. Hopker, M. Spira, and P. Zerwas, *Squark and gluino production at hadron colliders*, Nucl.Phys. **B492** (1997) 51–103, arXiv:hep-ph/9610490 [hep-ph].

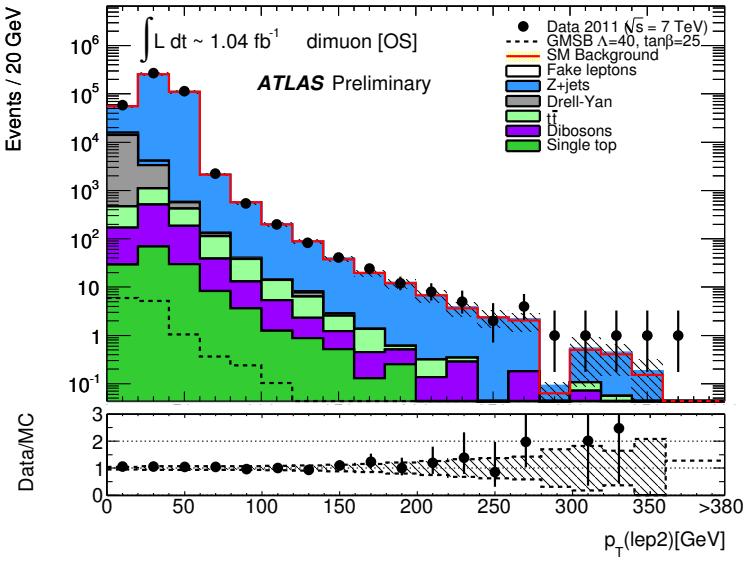

Figure 9: Distribution of the transverse momentum of the second leading muon after requiring two oppositely charged muons. The hatched bands reflect the statistical and systematic uncertainties. The expected contribution from a GMSB signal with $\Lambda = 40$ TeV and $\tan\beta = 25$ is also shown as a black dashed line.

[21] W. Beenakker, M. Kramer, T. Plehn, M. Spira, and P. M. Zerwas, *Stop production at hadron colliders*, Nucl. Phys. **B515** (1998) 3–14, arXiv:hep-ph/9710451 [hep-ph].

[22] W. Beenakker, M. Klasen, M. Kramer, T. Plehn, M. Spira, et al., *The Production of charginos / neutralinos and sleptons at hadron colliders*, Phys.Rev.Lett. **83** (1999) 3780–3783, arXiv:hep-ph/9906298 [hep-ph].

[23] M. Spira, *Higgs and SUSY particle production at hadron colliders*, arXiv:hep-ph/0211145 [hep-ph].

[24] T. Plehn, *Measuring the MSSM Lagrangean*, Czech. J. Phys. **55** (2005) B213–B220, arXiv:hep-ph/0410063 [hep-ph].

[25] P. M. Nadolsky, H.-L. Lai, Q.-H. Cao, J. Huston, J. Pumplin, et al., *Implications of CTEQ global analysis for collider observables*, Phys.Rev. **D78** (2008) 013004, arXiv:0802.0007 [hep-ph].

[26] ATLAS Collaboration, ATLAS-PHYS-PUB-2010-014 and ATLAS-CONF-2010-031.

[27] S. Agostinelli et al., Nucl. Instr. Meth. A **506** (2003) 250.

[28] ATLAS Collaboration, Eur. Phys. J. C **70** (2010) 823.

[29] G. S. M. Cacciari and G. Soyez JHEP **04** (2008) 063.

[30] ATLAS Collaboration, *Jet energy scale and its systematic uncertainty in proton-proton collisions at $\sqrt{(}s)$=7 TeV in ATLAS 2010 data*, ATLAS-CONF-2011-032.

[31] ATLAS Collaboration, Eur. Phys. J C **71** (2011) 1630 and ATLAS-CONF-2011-116.

[32] G. Cowan, K. Cranmer, E. Gross and 0. Vitells, Eur. Phys. J. C **71** (2011) 1554.

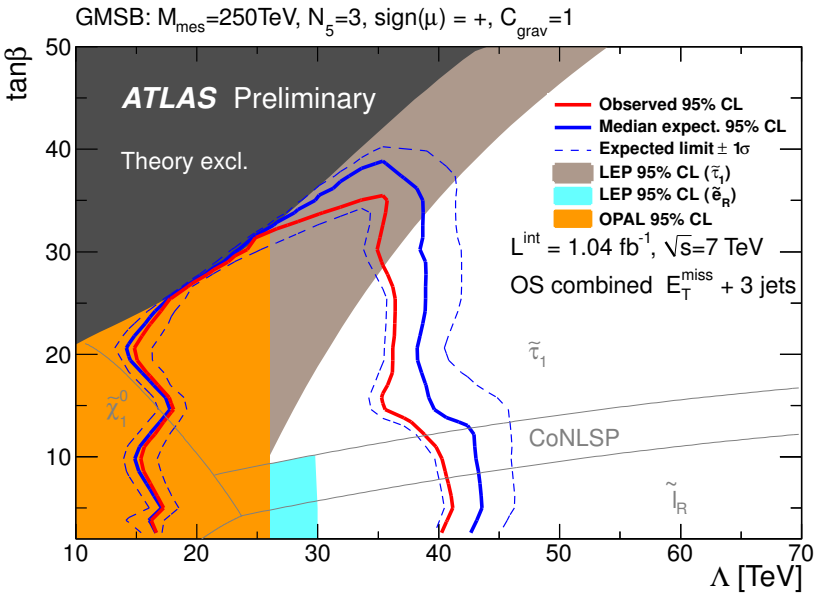

Figure 10: Observed (red) and expected (blue) 95% CL exclusion limits as function of Λ and $\tan\beta$ for the combination of all three channels. The $\pm 1\ \sigma$ lines (dashed) are also shown. The different NLSP regions as well as the region excluded by theory and LEP experiments are indicated as well. The limit contour in the region with values of Λ between 10 and 20 TeV is affected by limited MC statistics. The CoNLSP region denotes the phase space where $\tilde{\tau}_1$ and $\tilde{\ell}_R$ are nearly mass degenerate.

[33] A. Read, Journal of Physics G: Nucl. Part. Phys. **28** (2002) 2693-2704.